Optics Letters

Sub-two-cycle gigawatt-peak-power LWIR OPA for ultrafast nonlinear spectroscopy of condensed state materials

Vyacheslav Leshchenko,[1,2,*] Sha Li,[1] Pierre Agostini,[1] and Louis F. DiMauro[1]

[1]Department of Physics, The Ohio State University, Columbus, Ohio 43210, USA
[2]NeXUS Facility, Institute for Optical Science, The Ohio State University, Columbus, Ohio 43210, USA
*leshchenko.1@osu.edu

Received 14 July 2023; revised 23 August 2023; accepted 29 August 2023; posted 30 August 2023; published 18 September 2023

The application of high-power, few-cycle, long-wave infrared (LWIR, 8–20 μm) pulses in strong-field physics is largely unexplored due to the lack of suitable sources. However, the generation of intense pulses with >6 μm wavelength range is becoming increasingly feasible with the recent advances in high-power ultrashort lasers in the middle-infrared range that can serve as a pump for optical parametric amplifiers (OPA). Here we experimentally demonstrate the feasibility of this approach by building an OPA pumped at 2.4 μm that generates 93 μJ pulses at 9.5 μm, 1 kHz repetition rate with sub-two-cycle pulse duration, 1.6 GW peak power, and excellent beam quality. The results open a wide range of applications in attosecond physics (especially for studies of condensed phase samples), remote sensing, and biophotonics. © 2023 Optica Publishing Group

https://doi.org/10.1364/OL.500550

High-power and high-intensity femtosecond laser sources have been limited to $\lesssim$ 6 μm spectral range. However, the development of high-power ultrafast sources in the long-wave infrared range (LWIR, 8–20 μm) will enable a number of important fundamental studies and applications such as direct laser acceleration [1], high-energy particle and nuclear physics, studies of the breakdown of the dipole approximation [2], as well as remote sensing [3,4] and advanced molecular spectroscopy where the ability of LWIR to access vibrational resonances of molecules gives rise to sensitivity upon optical probing [5]. Moreover, high-power sources beyond 6 μm are essential for the study of fundamental properties of materials with low ionization potential, especially in the condensed state [6,7].

In this Letter, we experimentally demonstrate the feasibility of generating high-power LWIR pulses in a GaSe-based optical parametric amplifier (OPA) pumped with a middle-infrared (mid-IR) Cr:ZnSe laser at 2.4 μm [8]. The OPA delivers sub-two-cycle pulses at 9.5 μm central wavelength, 93 mW (93 μJ) with excellent beam quality and energy stability, which illustrates the advantage of the mid-IR pump lasers over the near-IR pump for LWIR generation and should stimulate further developments in this directions supported by the remarkable progress in mid-IR high-power optical systems in the last decade [8–11].

Traditionally, difference frequency generation (DFG) is the most compact and "simple" technique for LWIR generation, which is commercially available, but it is also very inefficient, especially when pumped at ~ 0.8–1 μm. For example, commercial systems with >10 mJ pulse energy deliver $\lesssim$ 10 μJ energy in the LWIR spectral range [14]. Note that it is typically an extension of an OPA that implements DFG between signal and idler, which has better conversion efficiency compared with direct intra-pulse DFG at ~ 0.8–1 μm. OPA and optical parametric chirped pulse amplification (OPCPA) can offer significantly higher conversion efficiency compared with a DFG configuration [15–22]. Although DFG and OPA are the same three-wave mixing process based on the second-order nonlinearity, DFG is typically assumed to be a single stage process with two strong input beams, while OPA is a (multistage) amplification of a weak seed beam by a strong pump pulse. Presently, the most common crystals for LWIR generation are: lanthanum gallium silicate (LGS) [15,19]; $BaGa_4S_7$ (BGS) [23]; $ZnGeP_2$, zinc-germanium diphosphide (ZGP) [16–18,22], and AgGaS, silver gallium sulfide. However, they are limited to the spectral range $\lesssim$ 10 μm due to material absorption at longer wavelength. Promising alternatives for the 10–18 μm range are GaSe, gallium selenide (GS) [21] and $AgGaSe_2$, silver gallium selenite (AGSe) [20] (see phase matching curves in Fig. 1). Both have similar transmission window up to 18 μm. GS has better nonlinear properties, namely twice larger effective nonlinearity and broader phase matching supporting more than octave bandwidth, which are the main reasons for adopting GS in this work. However, AGSe has other advantages, such as the possibility to be cut at any angle and anti-reflection coated, while it is presently impossible for GS due to its mechanical properties and state-of-the-art production capabilities. Despite advantages of GS and AGSe, there are very few OPA results beyond 9 μm [21], and they are limited to a very low power (<5 μJ), which is not enough for most of applications. Presently, there is only one OPCPA result with pulse energy exceeding 10 μJ [24], which profits from a mid-IR pump source similar to our work. However, our simpler OPA design has almost an order of magnitude higher peak power due to shorter pulse duration and higher pulse energy in a simpler OPA design. Note that, the relative simplicity of OPA design is based on the fact that it does not require active synchronization between pump and seed and dispersion management in the

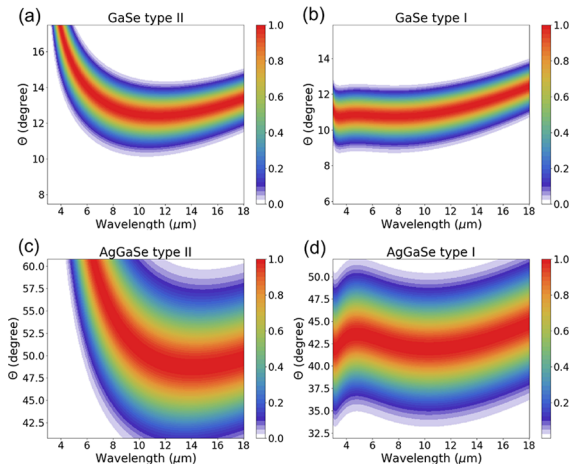

Fig. 1. Phase-matching-based low-signal gain at 2.4 μm pump wavelength as a function of the phase matching angle (Θ) and idler wavelength for (a) GaSe type II (o-signal, e-idler); (b) GaSe type I; (c) $AgGaSe_2$ type II (o-signal, e-idler); (d) $AgGaSe_2$ type I. The color scale is normalized to unity maximum value for every plot separately. Dispersion data from Refs. [12,13] is used in simulations.

stretcher and the compressor. The main reason for the lack of developments in the past is a quite strong linear and two-photon absorption of GS and AGSe in the most common pump range of 0.8–1μm.

Mid-IR pump lasers offer significant advantages over 0.8–1μm pump sources for LWIR OPAs for two main reasons: (i) overcoming the pump absorption problem mentioned above; (ii) fundamentally higher conversion efficiency in DFG and OPA applications due to the lower "quantum defect" (difference in photon energy between pump and idler photons, since the interaction is determined by the energy conservation $\hbar\omega_{\text{pump}} = \hbar\omega_{\text{signal}} + \hbar\omega_{\text{idler}}$). Thus, the maximum conversion efficiency is limited by the Manley–Rowe relation,

$$W_{\text{idler}}/\omega_{\text{idler}} = W_{\text{signal}}/\omega_{\text{signal}} = W_{\text{pump}}/\omega_{\text{pump}}, \quad (1)$$

where W is the power of the corresponding beam. Thus, smaller pump frequency (longer wavelength) is an obvious advantage. While advantages of mid-IR pumps have been experimentally proven for DFG applications [25,26], mid-IR-pumped OPAs are still in the infancy with very few and only low-power implementations [21].

Although nonlinear crystals suitable for LWIR OPAs have been available for a relatively long time, high-power ultrashort mid-IR pump sources became readily available only in the last years [8–11]. A few prominent examples are: Cr doped II-VI chalcogenides with ~ 2–3μm amplification spectral range [8,9]; Tm doped fiber lasers around 1.94 μm [10]; Er doped fibers at 2.8 μm [11]; Fe doped II-VI chalcogenides lasing in ~ 3–5μm range [9]. In this work we are using a Cr:ZnSe CPA system [8].

Our experimental setup is presented in Fig. 2. The pump beam has 2.4 μm central wavelength and 100 fs pulse duration (for more details see Ref. [8]). Approximately four percent (160 μJ) of the pump is split for seed generation via spectral broadening due to predominantly self-phase modulation [which is often called white light generation (WLG)]. The f-number of the focusing system in front of the WLG is 10. After testing a few different materials (CaF_2, BaF_2, and YAG), 4 mm undoped yttrium aluminum garnet (YAG) was identified as the best option

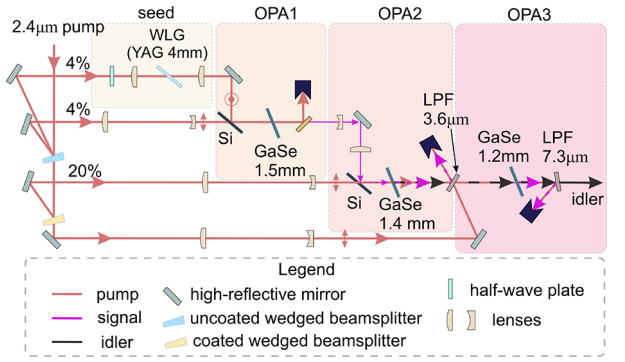

Fig. 2. Scheme of the experimental setup: LPF, long-pass filter; WLG, white-light generation.

with broad enough spectrum and high material damage threshold. In particular, no damaging of YAG occurs after weeks of operation, while BaF_2, despite more advantageous dispersion properties [27], gets damages after a few minutes, at least with standard commercially available polishing quality. Note that the wedge angle of the CaF_2 beam splitters shown in Fig. 2 is 0.5°, which do not affect the OPA performance, since it introduces negligible angular chirp of 6.5 μrad, which is just a couple percent of the beam divergence.

The preparatory numerical optimization of amplification stages was performed with the simulation system for optical science (Sisyfos) nonlinear wave propagation code [28], which includes most of the important linear and nonlinear processes. As a useful side note, after all experimental optimizations, we have identified that the effective nonlinearity is approximately 40% smaller compared with published results (although the data is available only for NIR pump pulses that is quite far from the 2.4 μm pump used in this work, which might explain the discrepancy, as well as crystal quality has some contribution to gain reduction for larger beams used in this work). Type II GS was chosen due to a slightly broader phase matching in 9–16 μm spectral range (see Fig. 1) and reduced Fresnel loss of idler on uncoated crystal surfaces. In addition, Type II effective nonlinearity is almost identical to Type I for GS.

All OPA stages are realized in the collinear geometry. The pump and the signal beams are combined with 1 mm-thick Si substrates at the Brewster's angle for the pump beam on the first and second stages. The Si substrates act as polarization combiners and cause almost no losses to the pump pulse and approximately 30% losses of the signal beam, which is not critical for the final performance due to the gain saturation on the last amplification stages. In the most common OPA design approach, the output of WLG, which corresponds to the "signal" beam, is consecutively amplified in all stages, while the longer wavelength "idler" beam, which is generated during the parametric amplification, is damped on all but the last stage. Here, we are using a more advanced approach enabling better performance of the idler beam. The idler beam in the ~ 7–14 μm spectral range generated in the second stage is amplified in the last stage, while the signal beam is damped after the second stage. This approach ensures better idler conversion efficiency, energy stability, and beam quality. For more details on comparison of signal versus idler amplification, see Ref. [29]. Between the second and the third stages, a hard coated reflective long-pass filter (LPF) is used for both removing the pump and the signal from the second stage and combining the idler from the second stage and the

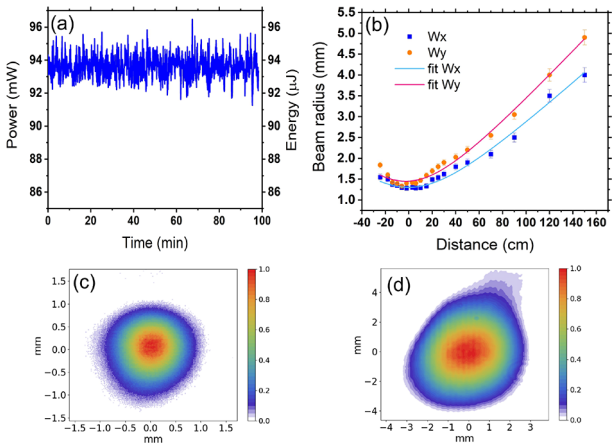

Fig. 3. (a) Output power stability. (b) Pulse quality (M-squared) measurement. Points are the measured beam size defined as the second moment width (D4σ), according to the ISO Standard 11146. Lines are the fits of the experimental data, based on which $M_x^2 = 1.1, M_y^2 = 1.3$. The range of negative distances was limited by the need to use reflective focusing optics (a spherical mirror) and adding a pair of wedges to reduce the power to a save level for the camera. (c) Beam profile at focus (0 cm distance). (d) Beam profile out of focus (120 cm distance).

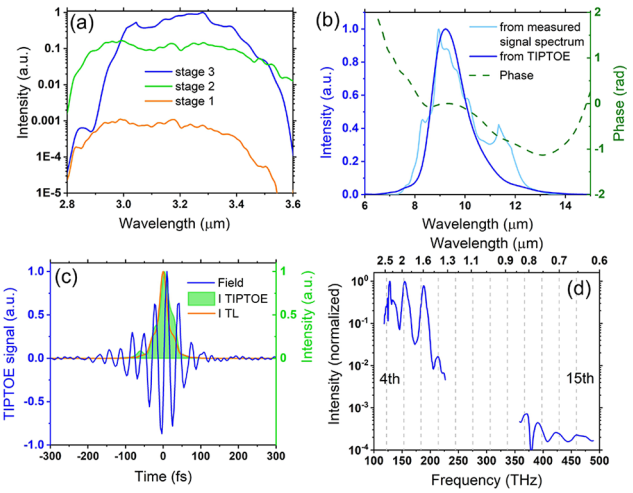

Fig. 4. (a) Signal spectrum measured after different amplification stages. (b) Reconstructed spectral intensity and phase. The light blue curve is the idler spectrum calculated from the signal spectrum measured after the third stage; the dark blue curve is the spectrum from the "time-domain observation of an electric field" (TIPTOE) measurement; the green curve is the phase reconstructed from the TIPTOE measurement. (c) TIPTOE signal corresponding to the pulse electric field (blue) and the reconstructed pulse intensity: filled green, reconstructed TIPTOE result; orange, transform limited (TL) pulse. (d) Spectrum of high-order harmonics generated in ZnTe. Vertical dashed lines identify expected positions of harmonics. The gap in the data is caused by the gap between the spectral ranges of the available spectrometers.

pump for the third stage. After amplification, signal and remaining pump are filtered out with another hard coated reflective LPF (extinction ratio >1000).

A pump energy of 4 mJ (4 W at 1 kHz) was used in this experiment, the idler average-power/energy is 93 mW/93 μJ with 0.7% root mean square (RMS) stability over a couple hours [see Fig. 3(a)], as measured with a thermal power detector UP19K from GENTEC-EO. No measurable background from the transmitted pump was detected after the last LPF. The pump power in the performed experiments was limited by the crystal size on the last stage, which has approximately 5 mm clear aperture (7 mm full aperture) for 4.5 mm e^2 beam diameters, and avoiding oversaturation that causes LWIR beam quality degradation without any gain in the output power. Note, a larger crystal, which is presently commercially available, will enable almost doubling of the output LWIR power by utilizing the full available 7 W of the pump beam. The output beam has good beam quality as presented in Fig. 3(b) with M-squared parameter of 1.1 and 1.3 for X and Y axes, respectively. The beam profile is measured with WinCamD-IR-BB camera from DataRay.

The signal spectrum was measured directly with a WaveScan APE spectrometer [see Fig. 4(a)], whereas the idler is outside of the spectrometer range. Nonetheless, it is possible to reconstruct the idler spectrum from the signal using the Manley–Rowe relation, Eq. (1). The result is presented in Fig. 4(b) (light blue curve). The amplified spectrum spans almost octave and corresponds to 35 fs full width at half maximum (FWHM) transform limited pulse duration, which is equivalent to slightly more than one optical cycle of 31.7 fs at the measured 9.5 μm central wavelength. The duration of the output pulse was measured with the TIPTOE technique [30] based on the visible band fluorescence emission in ZnSe in a home-built setup similar to Ref. [31]. The measured TIPTOE signal [Fig. 4(c)] corresponds to the pulse duration of 50 ± 5 fs, which is less than two optical cycles and together with measured energy corresponds to 1.6 GW peak power. The measured spectral phase is shown in Fig. 4(b) and can be, at least, partially compensated by introducing material, e.g., a pair of wedges. The advantage of LWIR spectral range is that transparent materials with both positive and negative group delay dispersion (GDD) are readily available (e.g., positive, Ge; negative, ZnSe and KBr). For example, adding 350 μm-thick Ge and 280 μm ZnSe substrates will compress the generated pulse down to 42 fs according to performed calculations. However, further compression down to the transform-limited duration is not possible without compensation of higher-order dispersion that cannot be controlled by adding material.

The generated LWIR pulses were refocused in a 300 μm-thick ZnTe crystal to verify the basic capability of producing strong-field high-order harmonic generation in condensed matter. The estimated on-target LWIR intensity was approximately 200 GW/cm^2. As presented in Fig. 4(d), NIR/visible harmonics up to 15th-order (650 nm) are generated, while the detection of higher orders was hindered by strong band-gap fluorescence signal at 560 nm. The longer-wavelength part of the data was measured with a NIRQuest-512 spectrometer (Ocean Optics); the shorter-wavelengths were detected with a TRIAX180 spectrometer from Jobin Yvon—SPEX with PI-MAX intensified CCD from Princeton Instruments. The plateau-like scaling of harmonic amplitudes is a clear indication of a non-perturbative nature of all but fourth harmonics, since perturbative harmonics efficiency has a substantial reduction with the harmonic order [32]. A more detailed discussion of these results goes beyond the scope of this Letter and will be a part of a following manuscript.

While the presented system is based on standard stock components from major optics vendors, which makes it cost effective, it leaves a large room for improvements and increase of the output power. For example, the LPF after the last amplification

stage is measured to introduce 27% losses. In addition, each surface of the uncoated GaSe crystals causes approximately 15% Fresnel-reflection losses (even for p-polarized pump and idler, as the phase matching angle is relatively far from the Brewster's angle). After taking into account these losses, the idler power on the OPA3 crystal exit is 160 mW, which corresponds to 4.7% idler efficiency and 20% signal+idler efficiency. All these losses can be mitigated in future by using anti-reflective coated AGSe crystals (unfortunately GaSe cannot be coated with the state-of-the-art technology) and optimized dichroic mirrors. Further increase of the pump intensity results in oversaturation and appearance of nonlinear degradation of pump pulse; thus, a significant scaling of the LWIR pulse energy will require longer pump pulses and OPCPA technology. No beam profile degradation indicating any significant thermal issues was observed in the performed experiments. In addition, no crystal degradation is observed after a few hundred hours of operation. Scaling of the average power of the LWIR output to a multi-watt level could be possible, but it will require active crystal cooling, and the feasibility analysis of such a system goes beyond the scope of this Letter.

Theoretically, the idler should have passive carrier-envelope phase (CEP) stability [33], but it is not automatically true in a real experiment [34], and we presently do not have the ability to measure it. However, CEP is a very important parameter for a sub-two-cycle pulse. Thus, it forms the natural agenda for follow up developments and studies.

In summary, we have demonstrated a high-power LWIR OPA pumped at 2.4 μm and generating 93 mW / 93 μJ pulses at 9.5 μm with sub-two-cycle duration and excellent beam quality. The essential capability of driving highly nonlinear processes is experimentally proven by observing high-order harmonics up to visible range in ZnTe and strong fluorescence in ZnSe in the TIPTOE setup (note that fluorescence photons have 20 times higher photon energy than the LWIR pulse). The results pave the way toward readily accessible high-power LWIR sources for strong-field studies of low-IP targets, e.g., solids, and molecular spectroscopy. It is important to note that all beams in the developed OPA setup: pump, signal, and idler, are in atmospheric transmission windows, which makes the combination of the Cr:ZnSe laser and the GaSe (or AGSe) OPA a unique broadband ultrafast source for advanced remote sensing and spectroscopy applications in atmosphere.

Funding. Air Force Office of Scientific Research (FA-9550-15-1-0037); U.S. Department of Energy (DE-FG02-04ER15614); U.S. National Science Foundation (1935885).

Acknowledgments. The authors acknowledge Gunnar Arisholm for support in performing simulations for OPA optimization.

Disclosures. The authors declare no conflicts of interest.

Data availability. Data underlying the results presented in this paper are not publicly available at this time but may be obtained from the authors upon reasonable request.

REFERENCES

1. I. Jovanovic, G. Xu, and S. Wandel, Phys. Procedia **52**, 68 (2014).
2. H. R. Reiss, Phys. Rev. Lett. **101**, 043002 (2008).
3. B. M. Walsh, H. R. Lee, and N. P. Barnes, J. Lumin. **169**, 400 (2016).
4. S. Yakovlev, O. Romanovskii, S. Sadovnikov, D. Tuzhilkin, A. Nevzorov, O. Kharchenko, and N. Kravtsova, Results in Optics **8**, 100233 (2022).
5. K. V. Kepesidis, M. Bozic-Iven, M. Huber, N. Abdel-Aziz, S. Kullab, A. Abdelwarith, A. Al Diab, M. Al Ghamdi, M. A. Hilal, M. R. K. Bahadoor, A. Sharma, F. Dabouz, M. Arafah, A. M. Azzeer, F. Krausz, K. Alsaleh, M. Zigman, and J.-M. Nabholtz, BMC Cancer **21**, 1287 (2021).
6. Z. Wang, H. Park, Y. H. Lai, J. Xu, C. I. Blaga, F. Yang, P. Agostini, and L. F. DiMauro, Nat. Commun. **8**, 1686 (2017).
7. M. R. Bionta, E. Haddad, A. Leblanc, V. Gruson, P. Lassonde, H. Ibrahim, J. Chaillou, N. Émond, M. R. Otto, A. Jiménez-Galán, R. E. F. Silva, M. Ivanov, B. J. Siwick, M. Chaker, and F. M. C. Légaré, Phys. Rev. Res. **3**, 023250 (2021).
8. V. E. Leshchenko, B. K. Talbert, Y. H. Lai, S. Li, Y. Tang, S. J. Hageman, G. Smith, P. Agostini, L. F. DiMauro, and C. I. Blaga, Optica **7**, 981 (2020).
9. S. B. Mirov, I. S. Moskalev, S. Vasilyev, V. Smolski, V. V. Fedorov, D. Martyshkin, J. Peppers, M. Mirov, A. Dergachev, and V. Gapontsev, IEEE J. Sel. Top. Quantum Electron. **24**, 1 (2018).
10. T. Heuermann, Z. Wang, M. Lenski, M. Gebhardt, C. Gaida, M. Abdelaal, J. Buldt, M. Müller, A. Klenke, and J. Limpert, Opt. Lett. **47**, 3095 (2022).
11. J. Huang, M. Pang, X. Jiang, F. Köttig, D. Schade, W. He, M. Butryn, and P. S. J. Russell, Optica **7**, 574 (2020).
12. K. Kato, F. Tanno, and N. Umemura, Appl. Opt. **52**, 2325 (2013).
13. H. Komine, J. Fukumoto, W. Long, and E. Stappaerts, IEEE J. Sel. Top. Quantum Electron. **1**, 44 (1995).
14. Light Conversion, "TOPAS," https://lightcon.com/product/topas-prime-high-energy-opa/#ufs.
15. M. Seidel, X. Xiao, S. A. Hussain, G. Arisholm, A. Hartung, K. T. Zawilski, P. G. Schunemann, F. Habel, M. Trubetskov, V. Pervak, O. Pronin, and F. Krausz, Sci. Adv. **4**, 1526 (2018).
16. D. Sanchez, M. Hemmer, M. Baudisch, S. L. Cousin, K. Zawilski, P. Schunemann, O. Chalus, C. Simon-Boisson, and J. Biegert, Optica **3**, 147 (2016).
17. U. Elu, T. Steinle, D. Sánchez, L. Maidment, K. Zawilski, P. Schunemann, U. D. Zeitner, C. Simon-Boisson, and J. Biegert, Opt. Lett. **44**, 3194 (2019).
18. S. Cheng, G. Chatterjee, F. Tellkamp, T. Lang, A. Ruehl, I. Hartl, and R. J. D. Miller, Opt. Lett. **45**, 2255 (2020).
19. B.-H. Chen, E. Wittmann, Y. Morimoto, P. Baum, and E. Riedle, Opt. Express **27**, 21306 (2019).
20. O. Novák, P. R. Krogen, T. Kroh, T. Mocek, F. X. Kärtner, and K.-H. Hong, Opt. Lett. **43**, 1335 (2018).
21. K. Liu, H. Liang, L. Wang, S. Qu, T. Lang, H. Li, Q. J. Wang, and Y. Zhang, Opt. Lett. **44**, 1003 (2019).
22. S. Wandel, M.-W. Lin, Y. Yin, G. Xu, and I. Jovanovic, Opt. Express **24**, 5287 (2016).
23. Z. Heiner, V. Petrov, and M. Mero, Opt. Lett. **45**, 5692 (2020).
24. P. Fuertjes, M. Bock, L. von Grafenstein, D. Ueberschaer, U. Griebner, and T. Elsaesser, Optica **9**, 1303 (2022).
25. K. Liu, H. Liang, S. Qu, W. Li, X. Zou, Y. Zhang, and Q. J. Wang, Opt. Express **27**, 37706 (2019).
26. C. Gaida, M. Gebhardt, T. Heuermann, F. Stutzki, C. Jauregui, J. Antonio-Lopez, A. Schülzgen, R. Amezcua-Correa, A. Tünnermann, I. Pupeza, and J. Limpert, Light: Sci. Appl. **7**, 94 (2018).
27. S. A. Frolov, V. I. Trunov, V. E. Leshchenko, and E. V. Pestryakov, Appl. Phys. B **122**, 124 (2016).
28. G. Arisholm, J. Opt. Soc. Am. B **14**, 2543 (1997).
29. S. Tóth, R. Flender, B. Kiss, M. Kurucz, A. Andrianov, R. S. Nagymihaly, L. Haizer, E. Cormier, and K. Osvay, J. Opt. Soc. Am. B **36**, 3538 (2019).
30. S. B. Park, K. Kim, W. Cho, S. I. Hwang, I. Ivanov, C. H. Nam, and K. T. Kim, Optica **5**, 402 (2018).
31. Y. Liu, S. Gholam-Mirzaei, J. E. Beetar, J. Nesper, A. Yousif, M. Nrisimhamurty, and M. Chini, Photonics Res. **9**, 929 (2021).
32. J. Wildenauer, J. Appl. Phys. **62**, 41 (1987).
33. A. Baltuška, T. Fuji, and T. Kobayashi, Phys. Rev. Lett. **88**, 133901 (2002).
34. N. Thiré, R. Maksimenka, B. Kiss, C. Ferchaud, P. Bizouard, E. Cormier, K. Osvay, and N. Forget, Opt. Express **25**, 1505 (2017).

340.254.107.208 ps 2023-10-18 11:45:07